Fundamental Limits to Wavefront Sensing in the Submillimeter

E. Serabyn
Jet Propulsion Laboratory, California Institute of Technology,
4800 Oak Grove Drive, Pasadena, CA, USA 91109

ABSTRACT

With the advent of large-format submillimeter wavelength detector arrays, and a new 25 m diameter submillimeter telescope under consideration, the question of optimal wavefront sensing methods is timely. Indeed, not only should bolometric array detectors allow the use of a variety of wavefront sensing techniques already in use in the optical/infrared, but in some cases it should actually be easier to apply these techniques because of the more benign temporal properties of the atmosphere at long wavelengths. This paper thus addresses the fundamental limits to wavefront sensing at submillimeter wavelengths, in order to determine how well a telescope surface can be measured in the submillimeter band. First several potential measurement approaches are discussed and compared. Next the theoretical accuracy of a fringe phase measurement in the submillimeter is discussed. It is concluded that with Mars as the source, wavefront sensing at the micron level should be achievable at submillimeter wavelengths in quite reasonable integration times.

Keywords: Submillimeter Wavefront Sensing

1. INTRODUCTION

With new and potential millimeter/submillimeter telescopes either in the planning phase or having recently starting operation, it is a good time to address the question of the fundamental limit to the accuracy with which a submm telescope's surface can be measured. Interestingly, while a number of wavefront sensing techniques have been applied to mm/submm telescopes in the past, the question of the ultimate sensitivity of these techniques is rarely formally addressed. Indeed, the common approach is to improve the performance of a given wavefront sensing technique only until it meets a particular telescope's needs. On the other hand, with a new 25 m submm telescope (CCAT – the Cornell Caltech Atacama Telescope; these proc.) being considered, it is important to determine how accurately such a telescope can be made, and in particular, how accurately the surface can be measured.

On the other hand, a new measurement technique might also be beneficial to already established submm telescopes, as it might allow more efficient operation at higher frequencies. To date, a number of different surface measurement techniques have been applied at various millimeter and submm telescopes, with the best measurement accuracies achieved to date being of order 7 – 10 μm, and resultant telescope accuracies of order 10 – 30 μm. With the opening of the Atacama plateau to submm telescopes, even higher frequencies are becoming accessible, which call for even higher surface accuracies. Figure 1, which plots the aperture efficiency vs. rms surface accuracy, shows the large gains in sensitivity which can be brought about by improved telescope performance.

At the same time, submillimeter detector arrays have become available over the past several years, while most submm wavefront sensing techniques continue to utilize single-pixel detectors (excluding phase reconstruction). On the other hand, array-based wavefront sensing techniques are standard practice in the optical/infrared regime, and so one of these shorter-wavelength techniques might conceivably find application in the submm regime. Therefore it is fair to ask whether submm arrays can enable new submm wavefront sensing techniques.

Of course, for any technique, many questions about specifics remain, such as the question of the optimal wavelength to use for the measurement. Indeed, one of the basic questions is whether to measure a telescope surface within the nominal telescope operating passband or not. Thus before addressing the fundamental performance limits to wavefront sensing in the submm, it is necessary first to discuss a few background issues.

2. BACKGROUND ISSUES

2.1 Why sense in the observing passband?

For any telescope, the mechanical model of the surface usually requires empirical verification and calibration. For example, Figure 2 shows a comparison of measurements and theoretical predictions for the elevation angle dependence of the CSO surface[1]. While the shapes are similar, the magnitudes of the deviations differ by about a factor of 2.

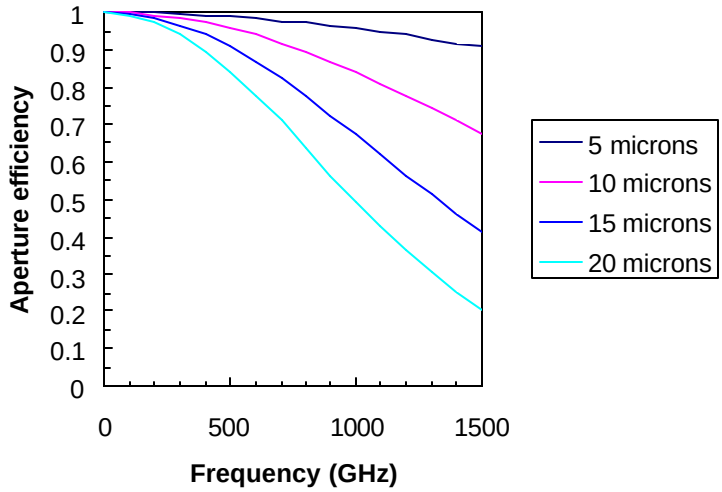

Fig. 1. Aperture efficiency vs. wavelength for different telescope rms surface accuracies.

At the same time, while local sensors such as metrology or edge sensors can be used to maintain a given telescope surface shape stably, it is still necessary to determine which shape to hold. For this it is necessary to use a technique which samples the full telescope surface, rather than a number of localized spots. Thus it is desirable to use the reflection of the actual telescope beam off of the dish surface as the ultimate descriminator.

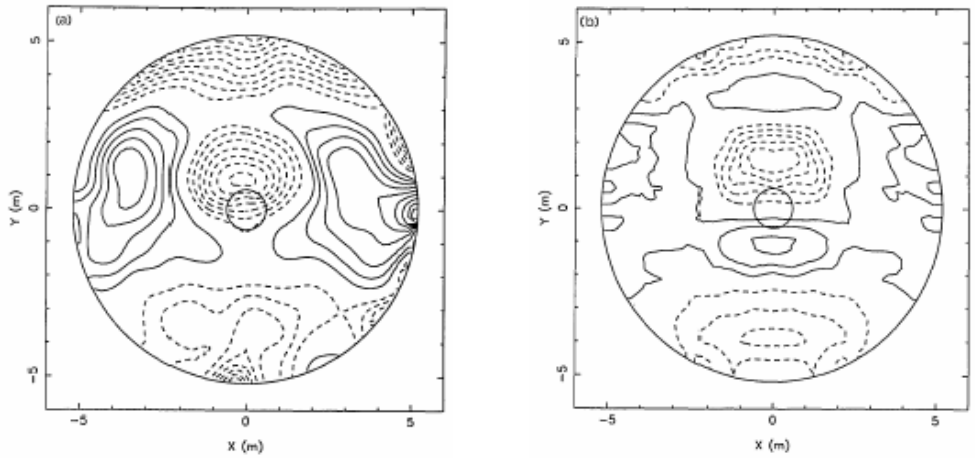

Fig. 2. Comparison[1] of CSO surface measurements (left) and model (right). The contour interval is 10 microns.

Although in principle any wavelength longer than the rms surface accuracy could be used, a wavelength within the telescope's operating passband provides absolute truth, and also has the advantage that a facility detector can perhaps be used as the detecting element. Of course, facility instrumentation typically provides aperture efficiency measurements at observing wavelengths, but aperture efficiencies provide only rms surface knowledge through the Ruze/Strehl formula, and not a map of the dish surface. On the other hand, wavefront sensing at a wavelength within the observatory's design passband provides a complete optical system performance test of the full primary plus secondary optical beam train.

2.2 Goals/requirements for a submm wavefront sensor

The goals for a submm wavefront sensor for a high-performance submm telescope can be summarized as follows:

- WFS accuracy: a small contributor to the error budget: a few (≤ 3) μm
- Lateral resolution:
  - – secondary decenter and focus: several points per telescope, e.g. 8×8 map
  - – gravitational flexure: ≈1 point per panel, e.g. 16×16 map
  - – panel shapes: few points per panel, e.g. 32×32 to 64×64 maps
- Time resolution: small (5-10°) elevation angle range, e.g. < 1 hr
- Measurement wavelength: use of a facility detector, e.g. 0.3 to 3 mm
- Measurement interval: occasional, e.g. a few months

2.3 Wavelength issues

Several factors enter into the determination of the optimal wavelength:

- Dish surface errors are more prominent at shorter wavelengths
- Atmospheric transmission generally degrades to shorter wavelengths
- The beam width decreases to shorter wavelengths

  ⇒ Need smaller sources (smaller than λ/D) for high frequency measurements
- Source signal: photons from thermal sources such as the planets increase to shorter wavelengths
- Photon bunching noise decreases to shorter wavelengths
- Field of view (FOV) and optics size decrease to shorter wavelengths

  e.g., FOV = $NF\lambda \approx (200 - 500)\lambda$ for F = 10 and N = 20 – 50

2.4 Source issues

The need for high signal to noise ratio (SNR) limits the available astronomical sources to the planets. However, the source diameter needs to be $< \lambda/D$ to allow for measurements out to the dish edge. Because for a 25 m telescope the beamwidth ranges from 12" at 1.5 mm to 2.4" at 300 microns, the only planets which remain as viable possibilities are Mars, Uranus and Neptune. Indeed, even Mars can only be used for such large telescope diameters when it is at the lower end of its angular diameter range.

Of course in the pupil plane the relevant metric is the source flux per measurement subaperture. Thus, larger telescope diameters do not provide any advantage in terms of signal per subaperture. Luckily, Mars emits a large flux – in particular, if Mars is observed at a wavelength where its angular diameter matches λ/D, its number flux density is $\approx 10^9$ photons/s/m^2, independent of wavelength across the submm. Thus signal is not an issue for Mars. What is an issue is the limited number of other bright sources available, since Mars is not available year-round, and is too large at opposition.

2.5 Background and noise issues

While point by point measurement approaches based on the use of a single detector pixel are time consuming, and more subject to corruption by fluctuations than instantaneous pupil mapping approaches, a single pixel detector has the advantage that it only accepts a limited number of modes of background radiation. On the other hand, all array-based approaches accept a correspondingly larger ($\approx N^2$) number of background modes.

2.6 Assumptions

In order to proceed quickly, the following assumptions are made here:

- Wavefront sensing is carried out within the telescope's design passband
- Only direct detection approaches are considered here. (Heterodyne techniques have good sensitivity because of the strength of nearby transmitters, but are typically limited to a single low elevation angle (in some cases $< 0°$)
- The noise is background limited
- Each detector pixel accepts roughly one mode of background radiation.

3. POTENTIAL SUBMM WAVEFRONT SENSING APPROACHES

Wavefront sensing can be carried out in the focal plane or the pupil plane, but since a Fourier transform connects the two, this is not an essential discriminator. Past approaches at mm/submm wavelengths have all relied on focal-plane measurements, and so focal plane approaches are the starting point here.

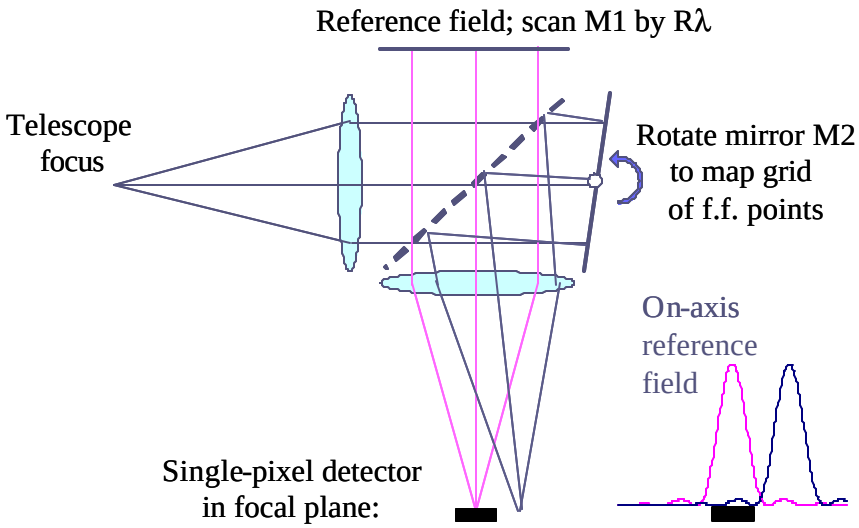

Fig. 3. Focal plane shearing interferometry[1]. Two telescope images are generated on the two flat mirrors in a Michelson interferometer. The core of the point spread function (PSF) from one of the two interferometer arms is used as a reference field on a single pixel detector, and the PSF from the other interferometer arm is sheared relative to the reference field by rotating mirror M2. N x N off-axis far-field (f.f.) points forming a regular grid are sequentially mapped onto the detector, and at each position, the optical path difference is scanned by Rλ.

3.1 Point by point focal plane shearing interferometry

The focal plane shearing interferometry approach (Fig. 3) implemented at the CSO[1,2] uses a single-pixel detector to sequentially measure the complex electric field at each of N x N points in the focal plane. At each off-axis point, in order to separate sidelobes at different wavelengths, an optical path difference (OPD) of length $R\lambda$ must be scanned, where $R = \lambda/\Delta\lambda$ is of the order of N. Therefore approximately N^3 data points must be acquired sequentially. However, only one spatial mode of background radiation is detected because a single pixel detector is used.

3.2 Wide-field focal plane interferometry

The main limitation of the shearing interferometry approach is that the reference field is concentrated into a single spatial pixel of size λ/D, leading to the need for sequential point by point measurements. One might thus consider expanding the reference field to cover the entire N x N region of interest in the focal plane. This could be done with e.g., a point diffraction interferometer[3] (PDI), in which the light in one arm of a Mach-Zehnder interferometer traverses a small pinhole, as in Figure 4. The core of the point spread function is spatially filtered by the pinhole and then collimated to provide a uniform reference field. The other arm of the interferometer provides the focal plane field. An array detector can then be used to measure the entire focal plane field simultaneously. Here again the OPD must be scanned by $R\lambda$ to resolve sidelobes at different wavelengths.

However, because the reference beam power is now distributed over N^2 spatial pixels, the expanded reference field is lower by roughly 1/N, as is the signal (the product of the reference and off-axis fields) in each pixel. Because each pixel receives its own mode of background radiation, each pixel's SNR (instantaneous or single scan) is then lower by 1/N as well. However, by accumulating N^2 scans in OPD, the SNR in each pixel can be restored to its value in the focal plane shearing approach. As these scans take N^2 longer in time than a single OPD scan, this approach yields the same net SNR as single-pixel focal-plane shearing interferometry (which also uses N^2 OPD scans) in the same total integration time. However, systematics are likely improved, because the entire pupil plane field is measured simultaneously. Indeed, with spatial mapping motions eliminated completely, time savings due to overhead reduction are possible as well. Finally, note that the same sensitivity analysis applies to any method used to broaden the reference field – the field and the SNR per pixel are reduced by 1/N.

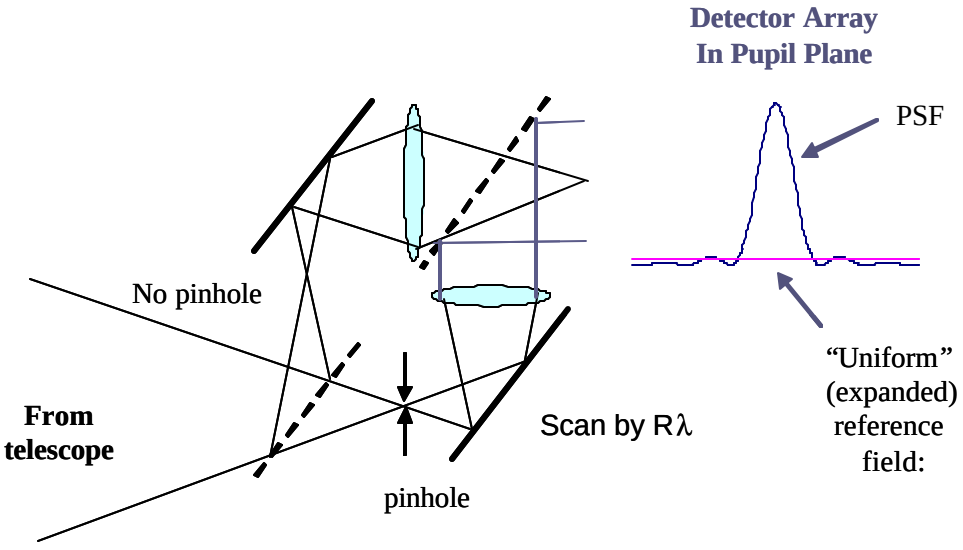

Fig. 4. Focal plane measurements with an expanded reference field. The spatially-filtered arm of the PDI provides a broad reference field, so that the entire focal-plane field distribution can be measured simultaneously. OPD scans of $R\lambda$ are still required to separate sidelobes.

3.3 Dispersed-fringe focal-plane shearing interferometry

It is also possible to modify the focal-plane shearing interferometer approach by using a spectrometer after the shearing interferometer to disperse the light in the single spatial pixel undergoing measurement (Fig. 5). In this case, the phase measurement of an off-axis point only needs an OPD scan of λ rather than $R\lambda$. In the background limit and the same total integration time, the SNR produced by a dispersive spectrometer utilizing a line array is higher than that resulting from Fourier transforming a single scan in OPD by the square root of the ratio of the noise (background) bandwidth to the spectral channel width[4]. Thus in equal integration times, the map SNR in this dispersed fringe approach is higher by the same ratio. With typical parameters, e.g., a total bandwidth of 80 GHz and a spectral channel width of order 10 GHz, the final map SNR is then higher by about a factor of 3 when dispersing the light. In addition, systematics could be lowered by taking fewer OPD scans per visit at each position, allow for more rapid individual map completion.

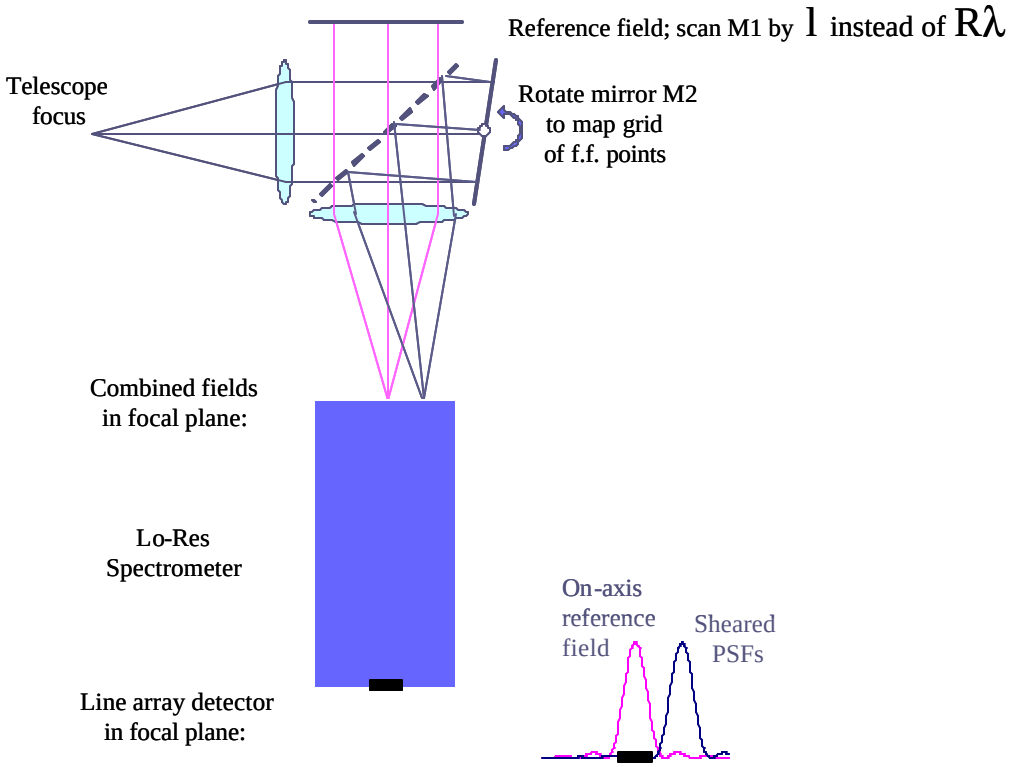

Fig. 5. Dispersed-fringe focal plane shearing interferometry. Here the Michelson interferometer is followed by a grating spectrometer. Each of the N x N off-axis positions is still measured sequentially. The optical path difference is now only scanned by λ, because the spectrometer separates the sidelobes at different wavelengths.

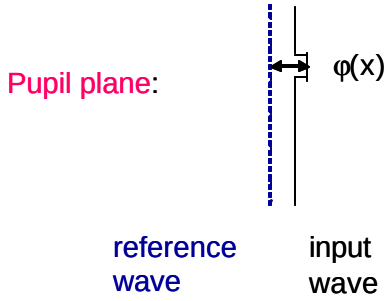

Fig. 6. Schematic of a pupil plane phase measurement.

3.4 Pupil plane measurements

Finally, with an array detector, measurements can be carried out directly in the pupil plane (Fig. 6), as is common laboratory practice in the optical/IR (with e.g. phase-shifting interferometry[5]). As in the last section, a PDI can again be used to generate a reference field (Fig. 7). However, to factors of order unity, in the background limit it doesn't matter which specific optical implementation is applied to obtain the measurements.

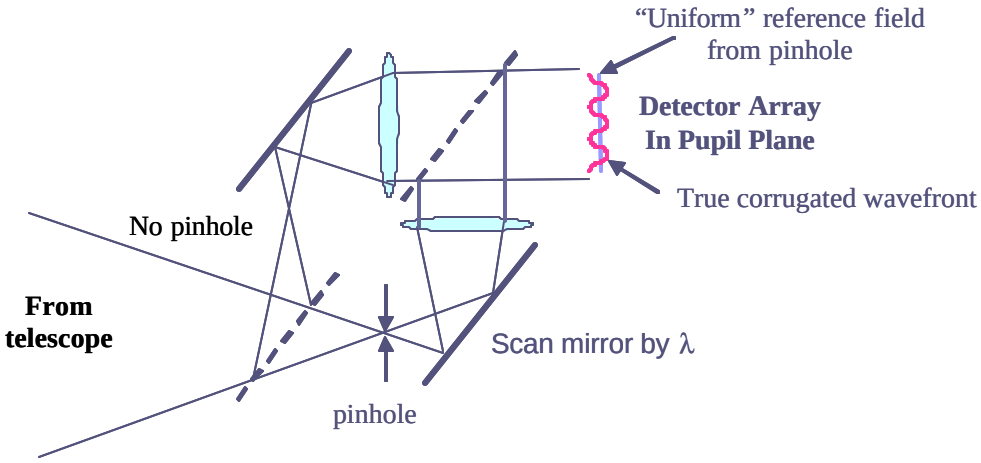

Fig. 7. Pupil plane interferometry. In this case, a reference wave is generated with a point-diffraction interferometer. An OPD scan of only λ is needed, because all wavelengths are in phase at the white light fringe position.

4. SENSITIVITY TO PUPIL PLANE PHASE

To calculate the sensitivity limit, it is most straightforward to consider pupil plane phase measurements (Fig. 6). As is well known, the rms phase accuracy, ϕ, of a fringe-based phase measurement is given by

$$f = \frac{1}{V \cdot SNR} \tag{1}$$

where V is the fringe visibility and *SNR* is the photometric SNR. Inserting the photometric quantities, this leads to

$$f = \frac{\sqrt{N_b}\sqrt{1+n}}{VN_s} \tag{2}$$

where N_s and N_b are the number of signal and background photons, respectively, in a measurement subaperture and measurement interval, and n is the occupancy number of the background mode.

Although each of the terms in Eqn. 2 deserves a lengthy discussion, space limitations demand brevity. Thus a number of simplifying assumptions will be applied. First, it is assumed that the visibility is somewhat less than unity, $V = 0.7$, and the emissivity, ε, is 0.5. Because these two factors enter as the ratio of the square root of the emissivity to the visibility, their exact values are not very important, as this ratio is within a factor of 2 of unity even if e.g., $\varepsilon \approx 0.3$ and $V = 1$. Next, the total transmission and the fractional bandpass are both assumed to be 10%. The factors in Eqn. 2 are then straightforward to calculate. With a 10% transmission and passband, the detected signal from Mars is $\approx 10^8$ photons per square meter per second, assuming as before that it is observed at a wavelength where its angular size is roughly equal to λ/D for a 25 m telescope. The background is of course much brighter, about 5×10^{11} photons per sec per mode for $\varepsilon = 0.5$. Inserting these numbers in Eqn. 2 then implies a phase accuracy in a square meter of

$$f \approx 0.01\sqrt{\frac{1+n}{t}} \text{ radians} \tag{3}$$

in measurement time t (in sec). Converting to rms surface error then gives

$$s \approx 1.6\times10^{-3}\, l\sqrt{\frac{1+n}{t}} \text{ radians,} \tag{4}$$

where λ is in microns. In the Rayleigh-Jeans limit, $n \approx kT/h\nu$, which for T = 273 K is equal to $56.8/\nu_{11}$, where ν_{11} is the frequency divided by 10^{11}. Thus, ignoring the frequency dependence of the atmospheric transmission spectrum, the measurement accuracy in the Rayleigh-Jeans limit theoretically degrades to longer wavelengths approximately as $\lambda^{3/2}$. On the other hand, the attainable accuracies are quite good across the submillimeter, of order 10 microns in a second at λ = 1.2 mm, and 2 microns in a second at λ = 350 μm. Including a factor of 2 for the time spent measuring an "off-source" map for background subtraction, the time needed to reach e.g., a 1-σ uncertainty of 1 μm over each square meter of telescope area is then about 3 min at 1.2 mm and 0.1 min at 350 μm.

These estimates are significantly shorter than the observing times achieved with the shearing interferometer at the CSO[1,2], implying that there is significant room for improvement. Indeed, overhead times in the CSO system (for far-field mapping moves, OPD scans, telescope moves and data transfer) are quite significant, leading to the prospect of significant improvement even with that single-pixel system.

5. SUMMARY

These initial sensitivity considerations are very encouraging. Based on photon statistics, it should be possible to reach significantly lower measurement errors than have been obtained to date. Furthermore, a number of techniques become available with detector arrays that can aid in reducing systematics. On the other hand, it should be possible to obtain improved performance even with the proven single-pixel shearing interferometry technique.

REFERENCES

1. E. Serabyn, T.G. Phillips and C.R. Masson, *Appl. Opt.* 30, 1127 (1989).
2. D. Woody, E. Serabyn and A. Schinkel, in Proc. SPIE 3357, 474 (1998).